

RSC Advances



This is an *Accepted Manuscript*, which has been through the Royal Society of Chemistry peer review process and has been accepted for publication.

Accepted Manuscripts are published online shortly after acceptance, before technical editing, formatting and proof reading. Using this free service, authors can make their results available to the community, in citable form, before we publish the edited article. This *Accepted Manuscript* will be replaced by the edited, formatted and paginated article as soon as this is available.

You can find more information about *Accepted Manuscripts* in the [Information for Authors](#).

Please note that technical editing may introduce minor changes to the text and/or graphics, which may alter content. The journal's standard [Terms & Conditions](#) and the [Ethical guidelines](#) still apply. In no event shall the Royal Society of Chemistry be held responsible for any errors or omissions in this *Accepted Manuscript* or any consequences arising from the use of any information it contains.

Coordination-resolved bonding and electronic dynamics of Na atomic clusters and solid skins

Maolin Bo,^a Yongling Guo,^a Yongli Huang,^a Yonghui Liu,^a YanWang,^{b*} Can Li,^c Chang Q Sun^{d*}

^aKey Laboratory of Low-Dimensional Materials and Application Technologies (Ministry of Education), Hunan Provincial Key Laboratory of Thin Film Materials and Devices, and School of Materials Science and Engineering, Xiangtan University, Hunan 411105, China

^bSchool of Information and Electronic Engineering, Hunan University of Science and Technology, Hunan 411201, China

^cInstitute of Coordination Bond Engineering, School of Materials Science and Engineering, China Jiliang University, Hangzhou 330018, China

^dNOVITAS, School of Electrical and Electronic Engineering, Nanyang Technological University, Singapore 639798, Singapore

*E-mail: ywang8@hnust.edu.cn, ecqsun@ntu.edu.sg

Abstract

Density functional theory calculations confirmed the bond-order-length-strength (BOLS) predictions regarding the local bond length, bond energy and electron binding energy (BE) of Na atomic clusters and shell-resolved monolayer skins. A reproduction of the photoelectron spectroscopic measurements leads to the following observations: (i) local lattice maximal strain of 14.51%, (ii) BE density of 71.92%, (iii) atomic cohesive energy of 62.31% and (iv) the $2p$ core-level shifts by 2.749 eV for under-coordinated Na atoms. This information helps in understanding the unusual behaviour of the under-coordinated Na solid skins and atomic clusters.

Keywords: Na solid skins and atom clusters, XPS, DFT, binding energy, BOLS

1. Introduction

Relaxation of bonds among under-coordinated atoms¹ at a solid skin and in an atomic cluster, their associated energies and the localization and polarization of electrons are of importance to the behaviour of materials at these atomic sites, such as crystal growth², adsorption³, doping⁴, decomposition⁵, catalytic reactivity⁶, work function⁷, etc. The relaxation of energy density⁸ and atom cohesive energy⁹ play significant roles, but are still less understood. Therefore, it is worth investigating under-coordinated atom systems to gain quantitative information regarding the coordination-resolved surface relaxation, binding energy (BE), and energy behaviour of electrons that are localised in the surface skin and nanoclusters.

In past study, X-ray photoelectron spectroscopy (XPS) was used in most studies on core-level shifts (CLS) of Na¹⁰⁻¹³, and the energy shifts were interpreted in terms of the difference in the energies between atoms on the surface and in the bulk body. Recently, free-electron laser ultraviolet (UPS) and XPS investigations of the Na¹⁴, K¹⁵, Rb¹⁶, Si¹⁷, Pb¹⁸, Au¹⁹, Se²⁰, Sb and Bi²¹ size-selected clusters revealed a linear dependence of the energy shifts of the core band on the inverse of the particle size. As the size decreases, nanoscale materials possess a non-negligible proportion of surface atoms, which can influence the properties of materials. For example, Alloyeau, *et al.* found that size and shape effects on the order–disorder phase transition in CoPt nanoparticles²². Billas, *et al.* found magnetism transition from the atom to the bulk in Fe, Co, and Ni clusters²³. Herzing, *et al.* found the identification of active Au nanoclusters on Fe oxide supports for CO oxidation²⁴. Therefore, determination of the physical mechanism behind the size dependency and size emergence of novel properties and the correlation among all the detectable properties is challenging.

Here, we show that the CLS of Na solid skins and atom clusters follow the predictions of the bond-order-length-strength (BOLS) notation and the tight-binding (TB) theory^{25,26}. A quantitative analysis using the density functional theory (DFT) and XPS spectrometric methods presents not only insight into the physical origin but also

the quantitative information on the electron BE in the skin and the clusters. The analysis also derives quantitative information of the local lattice strain, energy density, atomic cohesive energy and their effective coordination numbers.

2. Principles and calculation methods

2.1 BOLS -TB notation

According to the band theory, the Hamiltonian and the wave function describing an electron moving in the ν th orbit of an atom in the bulk solid is:

$$H = \left[-\frac{\hbar^2 \nabla^2}{2m} + V_{atom}(r) \right] + V_{cry}(r)(1 + \Delta_H).$$

The intra-atomic potential, $V_{atom}(r)$, determines the ν th core level energy, $E_\nu(0)$, of an isolated atom, and the crystal potential, $V_{cry}(r)$, determines the CLS, $\Delta E_\nu(z)$. They follow the relations:

$$\begin{aligned} E_\nu(0) &= \langle \nu, i | V_{atom}(r) | \nu, i \rangle \\ \Delta E_\nu(z) &= \langle \nu, i | V_{cry}(r)(1 + \Delta_H) | \nu, i \rangle \left[1 + \frac{z \langle \nu, i | V_{cry}(r)(1 + \Delta_H) | \nu, j \rangle}{\langle \nu, i | V_{cry}(r)(1 + \Delta_H) | \nu, i \rangle} \right] \\ &\cong E_b(1 + \Delta_H) \left(1 + \left(\frac{z\beta}{\alpha} < 3\% \right) \right) = E_z \end{aligned} \quad (1)$$

$|\nu, i\rangle$ is the eigenwave function at the i th atomic site with z neighbours, α is the exchange integral and β is the overlap integral. Because $\langle \nu, i | \nu, j \rangle = \delta_{ij}$, with the Kronig function δ_{ij} (if $i = j, \delta_{ij} = 1$; otherwise, $\delta_{ij} = 0$), E_b represents the single bond energy in the ideal bulk, and any perturbation to the bond energy E_b will shift the core level accordingly.

An extension of the atomic coordination-radius premise of Pauling²⁷ and

Goldschmidt²⁸ has resulted in the BOLS-TB notion, which forms the subject of²⁹. According to BOLS-TB notation, under-coordination shortens and strengthens the remaining bonds between the under-coordinated atoms, which follow the expressions:

$$\left\{ \begin{array}{l} C_z = d_z / d_b = 2 / \{1 + \exp[(12 - z_i) / 8z_i]\} \\ E_z = C_z^{-m} E_b \end{array} \right. , \quad (2)$$

Where C_z is the coefficient of bond contraction with z_i being the effective coordination of an atom in the i th atomic layer. The i counts from the outermost layer inward up to three. The bond-nature indicator m correlates the bond energy with the bond length. For most metals, $m = 1$. The coordination number (CN), i.e. $z = 0$ and $z = 12$, represent an isolated atom and an atom in the ideal bulk, respectively. Incorporating the BOLS into the TB approximation yields, dominates the shift of BE, and can be reorganised as follows:

$$\Delta E_v(z) = E_v(z) - E_v(0) = \Delta E_v(12)(1 + \Delta_i) = (E_v(12) - E_v(0))(1 + \Delta_H)$$

and,

$$\left\{ \begin{array}{l} \Delta_H = \sum_{i \leq 3} \gamma_i \Delta_i = \tau K^{-1} \sum_{i \leq 3} C_{z_i} \Delta_i = \tau K^{-1} \Delta'_H = \tau K^{-1} \sum_{i \leq 3} C_{z_i} (C_{z_i}^{-m} - 1) \quad (\text{Nanocluster}) \\ \Delta_i = \frac{E_z}{E_b} - 1 = C_{z_i}^{-m} - 1 \quad (\text{Solid skins}) \end{array} \right. \quad (3)$$

Here, $\sum_{i \leq 3} C_{z_i} \Delta_i = \Delta'_H$ and $\gamma_i = \tau C_{z_i} K^{-1}$ is the surface-to-volume ratio, proportional to τ ($\tau = 1, 2$, and 3 corresponds to the dimensionality of a thin plate, a cylindrical rod and a spherical dot, respectively), and inversely proportional to the dimensionless size K . $K = R/d_b$ is the number of atoms lined along the radius of a spherical nanoparticles. The Δ_H sums over only the outermost three atomic layers; the Δ_i represents the perturbation to the individual i th surface layer. For $i > 3$, the atomic bonds are assumed to be set sufficiently deep into the bulk of the solid such that they do not experience significant deficiencies in atomic coordination number (CN) unlike those at and near the surface.

Therefore, only the under-coordinated atoms in the surface skin contribute to the additional perturbation Δ_H to the overall Hamiltonian. The $\Delta_H(\tau, K^{-1}, m, z, d, E)$ covers all the possible extrinsic contributions from the shape(τ), size(K^{-1}) and the intrinsic contributions from bond nature(m), order(z), length(d) and energy(E) to the Hamiltonian. Chemical reaction or externally thermal and mechanical stimulations will modulate the m , d , and E values and hence the Hamiltonian.

2.2 Solid skins

According to the BOLS-TB notation, for the surface CLS we have the relation:

$$E_v(z) - E_v(0) = [E_v(12) - E_v(0)] \times C_z^{-m}$$

$$\frac{E_v(z) - E_v(0)}{E_v(z') - E_v(0)} = \frac{C_z^{-m}}{C_{z'}^{-m}} \quad (z' \neq z) \quad \text{or} \quad E_v(0) = \frac{C_{z'}^m E_v(z') - C_z^m E_v(z)}{C_{z'}^m - C_z^m} \quad (z' \neq z)$$
(4)

With the derived $E_v(12)$, $E_v(0)$, the bond-nature indicator m , and the given z values for the outermost three atomic layers, we are able to decompose the measured XPS spectra into the corresponding surface and bulk components.

The accuracy of Eq. (4) depends on the XPS calibration, which may not follow exactly the BOLS specification. Nevertheless, with this approach, one is able to elucidate, in principle, the dependence on CN of the core-level position of a material with all atomic CNs from $z = 0$ to $z = 12$. Therefore, the BOLS-TB approach uniquely defines the reference origin, the physical origin and the correlation between the core-level components for under-coordinated systems.

2.3 Nanocluster

Using the sum rule of the core-shell structure while taking the surface-to-volume ratio into effect, we can deduce the size dependence of v th energy level, $E_v(0)$, and its bulk shift, $\Delta E_v(12)$, as follows:

$$E_v(K) = E_v(12) + [E_v(12) - E_v(0)]\Delta_H \quad (5)$$

Generally, the size-induced BE shifts for nanoclusters depends inversely on the size in the form of, $E_v(K) = A + BK^{-1}$, where A and B are constants that can be determined by finding the intercept and the slope of the $E_v(K)$ line, respectively. Comparing the experimental scaling relationship with the theoretical expression in Eq. (5) yields:

$$\begin{cases} A = E_v(12) \\ B = [E_v(12) - E_v(0)]\tau \sum_{i \leq 3} C_{z_i} (C_{z_i}^{-m} - 1) \end{cases} \quad (6)$$

If a cluster is approximately spherical, the number of atoms N is related to its radius K by,

$$\begin{cases} K^{-1} = (3N / 4\pi)^{-1/3} = 1.61N^{-1/3} \\ N = 4\pi K^3 / 3 \end{cases} \quad (7)$$

The incorporation of Eq. (5), Eq. (6) and Eq. (7) yields the N -dependence of the core level binding energy³⁰:

$$E_v(N) = E_v(12) + \Delta E_v(12) \left[1.61\tau N^{-1/3} \sum_{i \leq 3} C_{z_i} (C_{z_i}^{-m} - 1) \right]. \quad (8)$$

For the detectable quantities can be directly connected to the bond identities such as bond nature(m), bond order(z), bond length(d), bond strength(E), we are able to predict the z -resolved local lattice strain(ϵ_z), the CLS($\Delta E_v(z)$), the atomic cohesive energy($\delta E_C(z)$) and the BE density($\delta E_D(z)$) follows the relation:

$$\begin{cases} \varepsilon(z) = C_z - 1 & \text{(local lattice strain)} \\ \Delta E_v(z) = \Delta E_v(12)C_z^{-m} & \text{(core level shift)} \\ \delta E_c(z) = z_{ib} C_z^{-m} - 1 & \text{(atomic cohesive energy)} \\ \delta E_d(z) = C_z^{-(m+3)} - 1 & \text{(binding energy density)} \end{cases} \quad (9)$$

Where $z_{ib} = z/12$ is the reduced CN, $z = 12$ is the bulk value and $m = 1$ for metal.

2.4 DFT calculation methods

In order to verify our BOLS-TB predictions, we conducted first-principle DFT calculations of the optimal Na_N clusters, as shown in **Fig. 1**. The calculations were focused on the change of the bond and electronic characteristics of under-coordinated atoms, geometric structures and size dependence and the energy distribution of the core band. The relativistic DFT calculations were conducted using the Vienna Abinitio simulation package (VASP). The DFT exchange-correlation potential utilised the local-density approximation (LDA)³¹ and generalised gradient approximation (GGA)³² for geometric and electronic structures. The plane wave cutoff was 350 eV; thus for refined structures, final and accurate energy values were computed by the same code using a precise cutoff energy of 400 eV in all the cases. A k-point sampling of $1 \times 1 \times 1$ Monkhorst–Pack grids in the first Brillouin zone of the cell was used in the calculation.

3. Results and discussion

3.1. Coordination-resolved solid skins

Fig. 2 shows a decomposition of the measured XPS $2p$ spectrum collected from a Na(110) surface¹⁰. The decomposition was conducted with reference to the CN values of a bcc(110) surface as the standard³³. The spectrum from surface of the Na(110) specimen was, respectively, decomposed into three components corresponding to the

bulk(B) and the surface skins S_2 and S_1 from higher(smaller absolute value) to lower BE after the background correction. These components follow the constraints of Eq. (4) and use the parameters given in **Table 1**. The BE of an isolated atom is optimised to be 28.194 eV with the respective bulk shift of 30.595 eV. The energies $E_v(0)$ and $E_v(12)$ should be identical for all the surface and subsurface layers of Na, regardless of the experimental or surface conditions. This decomposition shows that the undercoordination-induced BE shift is indeed positive and that the lowest coordination component shifts the most with respect to an isolated Na atom.

Including the common B component ($z = 12$) gives a total of $l = 3$ components for the Na(110) surface. A total, $N = C_l^2 = l! / [(l-2)!2!] = 3$, of values is possible for $E_v(0)$. Using the least root-mean-square approach, we can find the average $\langle E_v(0) \rangle = \sum_N \langle E_v(0) \rangle / N$ and standard deviation σ . To ensure minimum error in the envelope spectrum and in the experimental spectrum, we fine-tuned the z -values in the decomposition, obtaining an optimised z -value of 3.95 for the outermost (110) surface layer. Based on these criteria, we obtain the following z -resolved CLS for Na:

$$E_{2p}(z) = \langle E_{2p}(0) \rangle \pm \sigma + \Delta E_{2p}(12) C_z^{-m} = 28.194 \pm 0.006 + 2.401 C_z^{-1}.$$

This information is vital for understanding the physics of a Na (110) surface, such as skin-resolved quantum entrapment.

In addition, by using the z -dependent $2p$ BE shifts for each surface component as derived from XPS spectral decomposition, we can predict the z -resolved local lattice strain, the CLS, the atomic cohesive energy and the binding energy density for discrete atoms in the Na solid skins. Consistency between the BOLS predictions and the XPS derivatives has been achieved, as is shown in **Fig. 2b** and **Table 1**.

3.2 Coordination-resolved nanoclusters

Clusters have a considerable number of under-coordinated atoms that are located in the surface sites. **Fig. 3** shows the $2p$ -orbit density of states (DOS) of Na_{44} , Na_{46} , Na_{55A} and Na_{55B} clusters from which we obtain the BE and energy density evolution of atoms at

different sites. For a given CLS, from the relations in Eq. (2) and Eq. (3), we have the,

$$\begin{cases} z = 12 / \left\{ 8 \ln \left(\frac{2\Delta E_{2p}(z) - \Delta E_{2p}(12)}{\Delta E_{2p}(12)} \right) + 1 \right\} \\ E_{2p}(z) = \Delta E'_{2p}(z) + E(12) \text{ or } \Delta E_{2p}(z) = \Delta E'_{2p}(z) + \Delta E_{2p}(12) \end{cases} \quad (10)$$

$\Delta E_{2p}(z) = E_{2p}(z) - E_{2p}(0)$ and $\Delta E'_{2p}(z) = E_{2p}(z) - E_{2p}(12)$ are the CLSs of an isolated atom and an atom in the ideal bulk, respectively. Then, we calculate the atomic CN using Eq. (10). Comparing different atomic sites from i to j ($1 \leq i < j \leq 10$), the lower atomic CNs have larger BE shifts.

Fig. 4a shows a comparison of the derived CN and BE shifts at different atomic sites between different structures of Na: O_h44 , $C_{3v}46$, O_h55A and $C_{3v}55B$. We found atoms that have the same number of neighbour atoms and same BE shifts. For example, the third atom of Na_{44} , the third atom of Na_{46} , the second atom of Na_{55A} and the seventh and eighth atoms of Na_{55B} have the same CN and BE shifts. In addition, we compared the exchange correlation potentials of Na_{55B} calculated by LDA and GGA functions, as is shown in **Fig. 4b** and **Table 2**. The results of the calculations by the LDA and GGA functions are similar.

From **Figs. 3 and 4**, we evaluate the BE shift associated with the under-coordinated atoms. The effective CN is consistent with the energy effects at different atomic sites on the surface, which is an evidence of the sufficient accuracy of the derivatives. Therefore, solids and nanoclusters show the same effect: the under-coordinated atoms result in positive BE shifts and in skin-depth quantum entrapment. The concepts of quantum entrapment appear to be essential for understanding the bonding and electronic behaviour in surface and atomic defect sites.

3.3 N -dependence of nanoclusters

Fig. 5a shows DFT calculations of the $2p$ -orbit DOS for Na of I_h13 ,

$C_{125}, C_{2v30}, C_{2v32}$ and C_{2v53} clusters. DFT calculations showed that the peaks of BE shift toward higher binding energies as the cluster size is reduced. Therefore, a consistent understanding of the effect of the surface relation and nanosolid formation on the CLS is highly desirable.

In the BOLS convention, we choose the first and seventh atoms of Na_{55B} as the standard reference $CN(z)$ for the first and second atomic layers of the nanoclusters. Thus, we have $z_1 = 2.37$ and $z_2 = 5.39$. From the relation of $C(z_i)$ in Eq.(2), C_1 and C_2 were calculated to be 0.7514 and 0.9235, respectively. The sum $\Delta'_H = \sum_{i=3} C_{z_i} (C_{z_i}^{-m} - 1) = 0.3251$. With the value of $\Delta E_{2p}(12)$ derived from the surface analysis, we can calculate the BE change without the need for any other assumptions:

$$\begin{cases} E_{2p}(N) = E_{2p}^{Fermi}(12) + 1.257\tau N^{-1/3} \text{ (eV)} & \text{(Experimental)} \\ E_{2p}(N)' = E_{2p}(12)' + 1.257\tau N^{-1/3} \text{ (eV)} & \text{(Calculation)} \end{cases}$$

and,

$$\begin{cases} \Phi = E_{2p}^{Fermi}(12) - E_{2p}(12)' \text{ (eV)} \\ \Phi_1 = E_{2p}^{vacuum}(12) - E_{2p}^{Fermi}(12) \text{ (eV)} \end{cases}$$

(11)

Derived from the DFT calculation data, $\Delta E_{2p}(N)$ is mainly attributed to the size contribution. $\Phi_1 = 2.755$ eV is the work function^{10, 14} from vacuum to the Fermi level. $\Phi = 6.399$ eV is the bulk value difference between the DFT calculated value and the experimental value. **Fig. 5b** shows that the $2p$ core band CLS of size-selected free Na_N nanoclusters increases linearly with $N^{-1/3}$ and shape factor $\tau = 2.392$. According to the slope and intercept derived from size-induced BE shifts and Eq. (11),

$$\begin{cases} E_{2p}(N) = 30.595 + 3.007N^{-1/3} \text{ (eV)} & \text{(Experimental)} \\ E_{2p}(N)' = 24.196 + 3.007N^{-1/3} \text{ (eV)} & \text{(Calculation)} \end{cases}$$

As shown in **Fig. 5b**, the BOLS prediction is generally consistent with the core-level BE in both the experiment and the DFT calculation.

3.4 Cluster strain and CN imperfection

To obtain the nanocluster strain(ε_z) and the CN imperfection, we use the relations from the Eq. (8) and Eq. (10) and get:

$$\left\{ \begin{array}{l} z = 12 / \left\{ 8 \ln \left(\frac{2\Delta E'_{2p}(z) + \Delta E_{2p}(12)}{\Delta E_{2p}(12)} \right) + 1 \right\} \\ \Delta E'_{2p}(z) = E_{2p}(N)' - E_{2p}(12)' = 1.61\tau N^{-1/3} \sum_{i \leq 3} C_z (C_z^{-m} - 1) \end{array} \right. \quad (12)$$

For a given CLS $\Delta E'_{2p}(z)$, we have:

$$\left\{ \begin{array}{l} z = 12 / \left\{ 8 \ln \left(\frac{2.401 + 2 \times 3.007 N^{-1/3}}{2.401} \right) + 1 \right\} \\ \varepsilon_z = 2 / \left\{ 1 + \exp \left[(12 - z) / 8z \right] \right\} - 1 \end{array} \right. \quad (13)$$

Then, we calculate the N_{a_N} atomic CN and strain ε_z using Eq. (13)(see **Fig. 6** and **Table 3**).

Consistency between the BOLS-TB notation, DFT calculations and XPS measurements suggests that the observed energy shifts result from the size-induced strain and the associated skin-depth quantum trapping by nanoclusters or surface interlayer relaxation of a bulk solid, which agrees with the previously recommended mechanism of surface interlayer strain and charge densification³⁴⁻³⁶.

4. Conclusion

Combining the BOLS-TB premise with the DFT calculations and XPS measurements has led to the consistent insight into the physical origin of the localised edge states of the Na solid and cluster. Analysing the XPS spectrum of the Na(110) surface has resulted in the determination of the BE of an isolated atom as 28.194 eV, and its bulk shift as 2.401 eV. We have demonstrated the application of DFT calculation to the N -dependency of the core-level BE shifts, and to the quantitative analysis of atom

coordination numbers, local bond strain, energy density, atomic cohesive energy and their coordination-resolved shifts. In conclusion, we believe that our findings are useful for designing nanocrystals with desired structures and properties.

Acknowledgment

We acknowledge the financial support from NSF (Nos. 11172254 and 11402086).

Figure and Table captions:

Fig. 1 Geometrically optimised (a) O_h44 , $C_{3v}46$, O_h55A and $C_{3v}55B^{37}$; (b) I_h13 , C_{125} , $C_{2v}30$, $C_{2v}32$ and $C_{2v}53^{38,39}$ structures of Na clusters.

Fig. 2 (a) Decomposed XPS spectrum of the Na(110) surface¹⁰ with the three Gaussian components representing the bulk B and surface skins S_2 and S_1 . (b) Atomic cohesive energy δE_C and BE density δE_D . **Tables 1** and **2** show the derived information.

Fig. 3 DFT-derived DOS for (a) O_h44 , (b) $C_{3v}46$, (c) O_h55A and (d) $C_{3v}55B$ structures of Na clusters.

Fig. 4 Coordination number (z)-resolved CLS ($\Delta E'_{2p}(z) = E_{2p}(z) - \Delta E_{2p}(12)$) of Na clusters. (a) Comparisons of CLS among the results of DFT calculations for Na_{44} , Na_{46} , Na_{55A} and Na_{55B} with that of XPS measurements of Na_{3000} ⁴⁰. (b) A comparison of DFT calculations for a Na_{55B} atom (1-10) with LDA and GGA functions.

Fig. 5 (a) Size-induced quantum entrapment of Na_N clusters. (b) BE shift of size-selected free Na_N clusters versus $N^{-1/3}$. Experimental data of Na_{3000} , Na_{5000} and the bulk are sourced from the refs¹⁴.

Fig. 6 (a) Atomic CN and (b) strain ε_z versus $N^{-1/3}$ for Na nanoclusters.

Table 1 The effective CN(z), local lattice strain ($\varepsilon_z=(C_z-1)(\%)$), relative core-level shifts ($\Delta E_{2p}(z) = E_{2p}(z) - E_{2p}(0)$ and $\Delta E'_{2p}(z) = E_{2p}(z) - \Delta E_{2p}(12)$), relative atomic cohesive energy ($\delta E_C = (z_{ib} C_z^{-1} - 1)(\%)$) and the relative BE density ($\delta E_D = C_z^{-4} - 1(\%)$) in various registries of Na(110)¹⁰ surface.

	i	$E_{2p}(z)$	z	$\Delta E_{2p}(z)$	$\Delta E'_{2p}(z)$	$-\varepsilon_z$	$-\delta E_C$	δE_D
	Atom	28.194	0	---	---	---	---	---
	B	30.595	12	2.401	0	0	0	0
Na(110)	S ₂	30.764	5.83	2.570	0.169	6.61	47.98	31.43
	S ₁	30.943	3.95	2.749	0.348	12.67	62.31	71.92

Table 2 The average effective CN (z), relative core-level shifts ($\Delta E'_{2p}(z) = E_{2p}(z) - E_{2p}(12)$), relative atomic cohesive energy (δE_C) and the relative BE density (δE_D) in various registries of Na clusters.

	Atomic position	LDA			GGA			LDA	
		$E_{2p}(z)$	z	$\Delta E'_{2p}(z)$	$E_{2p}(z)$	z	$\Delta E'_{2p}(z)$	$-\delta E_C$	δE_D
Na ₄₄	1	25.382	2.37	0.794	25.407	2.58	0.697	73.715	213.756
	2	25.084	3.19	0.496	25.208	3.18	0.498	67.937	111.644
	3	24.787	5.39	0.199	24.909	5.39	0.199	51.363	37.482
	4	24.588	12	0	24.710	12	0	0	0
Na ₄₆	1	25.595	2.83	0.598	25.690	2.82	0.603	70.528	143.899
	2	25.395	3.65	0.398	25.488	3.63	0.401	64.549	84.534
	3	25.295	4.33	0.298	25.387	4.31	0.300	59.445	59.569
	4	25.196	5.39	0.199	25.286	5.39	0.199	51.363	37.482
	5	25.096	7.34	0.099	25.185	7.37	0.098	36.307	17.507
Na _{55A}	1	25.304	3.65	0.397	25.386	3.64	0.399	64.549	84.534
	2	25.106	5.39	0.199	25.187	5.37	0.200	51.363	37.482
	3	24.907	12	0	24.987	12	0	0	0
	1	25.626	2.37	0.796	25.642	2.56	0.703	73.715	213.756
	2	25.597	2.42	0.767	25.593	2.68	0.654	73.378	203.700
	3	25.542	2.54	0.712	25.568	2.75	0.629	72.499	184.500
	4	25.328	3.18	0.498	25.351	3.57	0.412	68.009	112.378
	5	25.228	3.65	0.398	25.340	3.63	0.401	64.549	84.534

Na _{55B}	6	25.129	4.32	0.299	25.240	4.30	0.301	59.521	59.853
	7	25.029	5.39	0.199	25.140	5.36	0.201	51.363	37.482
	8	25.029	5.39	0.199	25.140	5.36	0.201	51.363	37.482
	9	24.930	7.32	0.100	25.039	7.32	0.100	36.462	17.707
	10	24.830	12	0	24.939	12	0	0	0

Table 3 The cluster strain ($\varepsilon_z=(C_z-1)(\%)$) and relative core-level shifts ($\Delta E'_{2p}(z)=E_{2p}(N)'-E_{2p}(12)'$) from various registries of Na nanoclusters.

$$(\Phi_2 = E_{2p}^{vacuum}(12) - E_{2p}(12)')$$

	N	$E_{2p}(N)'$	$\Delta E'_{2p}(z)$	z	$-\varepsilon_z$
	13	25.421	1.225	1.81	33.80
Na cluster	25	25.214	1.018	2.02	29.93
(DFT)	30	25.157	0.961	2.10	28.64
	32	25.124	0.928	2.14	28.02
	53	24.979	0.783	2.39	24.61
Na cluster ¹⁴	3000	24.436	0.240	4.88	9.09
($\Phi_2=9.154$ eV)	5000	24.396	0.200	5.37	7.70
(Experimental)	Bulk	24.196	0	12	0

References

1. W. J. Huang, R. Sun, J. Tao, L. D. Menard, R. G. Nuzzo and J. M. Zuo, *Nature materials* **7** (4), 308-313 (2008).
2. Q. Wei, K. Tajima, Y. Tong, S. Ye and K. Hashimoto, *Journal of the American Chemical Society* **131** (48), 17597-17604 (2009).
3. M. a. M. Morgenstern, Thomas and Comsa, George, *Phys. Rev. Lett.* **77** (4), 703-706 (1996).
4. C.-L. Sun, C.-W. Pao, H.-M. Tsai, J.-W. Chiou, S. C. Ray, H.-W. Wang, M. Hayashi, L.-C. Chen, H.-J. Lin, J.-F. Lee, L. Chang, M.-H. Tsai, K.-H. Chen and W.-F. Pong, *Nanoscale* **5** (15), 6812-6818 (2013).
5. T. Kravchuk, L. Vattuone, L. Burkholder, W. T. Tysoe and M. Rocca, *Journal of the American Chemical Society* **130** (38), 12552-12553 (2008).
6. A. Bruma, F. R. Negreiros, S. Xie, T. Tsukuda, R. L. Johnston, A. Fortunelli and Z. Y. Li, *Nanoscale* **5** (20), 9620-9625 (2013).

7. C.-Y. Lin, H.-W. Shiu, L.-Y. Chang, C.-H. Chen, C.-S. Chang and F. S.-S. Chien, *The Journal of Physical Chemistry C* **118** (43), 24898-24904 (2014).
8. L. Wan, S. Xu, M. Liao, C. Liu and P. Sheng, *Physical Review X* **4** (1), 011042-011042 (2014).
9. J. Åberg, *Physical Review Letters* **113** (15), 150402-150402 (2014).
10. D. Riffe, G. Wertheim and P. Citrin, *Physical Review Letters* **67** (1), 116-119 (1991).
11. C. Su, X. Shi, D. Tang, D. Heskett and K. D. Tsuei, *Physical Review B* **48** (16), 12146-12150 (1993).
12. M. Tchapyguine, S. Legendre, A. Rosso, I. Bradeanu, G. Öhrwall, S. Canton, T. Andersson, N. Mårtensson, S. Svensson and O. Björneholm, *Physical Review B* **80** (3), 033405-033405 (2009).
13. T. Andersson, C. Zhang, A. Rosso, I. Bradeanu, S. Legendre, S. E. Canton, M. Tchapyguine, G. Öhrwall, S. L. Sorensen, S. Svensson, N. Mårtensson and O. Björneholm, *J Chem Phys* **134** (9), 094511-094511 (2011).
14. S. Peredkov, G. Öhrwall, J. Schulz, M. Lundwall, T. Rander, A. Lindblad, H. Bergersen, A. Rosso, W. Pokapanich, N. Mårtensson, S. Svensson, S. Sorensen, O. Björneholm and M. Tchapyguine, *Physical Review B* **75** (23), 235407-235407 (2007).
15. A. Rosso, G. Öhrwall, I. Bradeanu, S. Svensson, O. Björneholm and M. Tchapyguine, *Physical Review A* **77** (4), 043202-043202 (2008).
16. M. H. Mikkilä, M. Tchapyguine, K. Jänkälä, T. Andersson, C. Zhang, O. Björneholm and M. Huttula, *The European Physical Journal D* **64** (2-3), 347-352 (2011).
17. M. Vogel, C. Kasigkeit, K. Hirsch, A. Langenberg, J. Rittmann, V. Zamudio-Bayer, A. Kulesza, R. Mitrić, T. Möller, B. v. Issendorff and J. T. Lau, *Physical Review B* **85** (19), 195454-195454 (2012).
18. M. Tchapyguine, G. Öhrwall, T. Andersson, S. Svensson, O. Björneholm, M. Huttula, M. Mikkilä, S. Urpelainen, S. Osmekhin, A. Caló, S. Aksela and H. Aksela, *Journal of Electron Spectroscopy and Related Phenomena* **195**, 55-61 (2014).
19. A. Visikovskiy, H. Matsumoto, K. Mitsuahara, T. Nakada, T. Akita and Y. Kido, *Physical Review B* **83** (16), 165428-165428 (2011).
20. K. Kooser, D. T. Ha, E. Itala, J. Laksman, S. Urpelainen and E. Kukkk, *J Chem Phys* **137** (4), 044304-044304 (2012).
21. S. Urpelainen, M. Tchapyguine, M. H. Mikkilä, K. Kooser, T. Andersson, C. Zhang, E. Kukkk, O. Björneholm and M. Huttula, *Physical Review B* **87** (3), 035411-035411 (2013).
22. D. Alloyeau, C. Ricolleau, C. Mottet, T. Oikawa, C. Langlois, Y. Le Bouar, N. Braidy and A. Loiseau, *Nat Mater* **8** (12), 940-946 (2009).
23. I. M. L. Billas, A. Châtelain and W. A. de Heer, *Science* **265** (5179), 1682-1684 (1994).
24. A. A. Herzing, C. J. Kiely, A. F. Carley, P. Landon and G. J. Hutchings, *Science* **321** (5894), 1331-1335 (2008).
25. X. J. Liu, M. L. Bo, X. Zhang, L. T. Li, Y. G. Nie, H. Tian, S. Xu, Y. Wang and C. Q. Sun, *Chemical reviews* **Accepted 03/10/2014** (2014).
26. C. Q. Sun, Y. Nie, J. Pan, X. Zhang, S. Z. Ma, Y. Wang and W. Zheng, *RSC Advances* **2** (6), 2377-2383 (2012).
27. L. Pauling, *J Am Chem Soc* **69** (3), 542-553 (1947).
28. V. M. Goldschmidt, *Berichte Der Deutschen Chemischen Gesellschaft* **60**, 1263-1296 (1927).
29. C. Q. Sun, *Relaxation of the Chemical Bond*. (Springer, Heidelberg, 2014).

30. M. Bo, Y. Wang, Y. Huang, W. Zhou, C. Li and C. Q. Sun, *Journal of Materials Chemistry C* **2** (30), 6090-6096 (2014).
31. A. D. Becke, *The Journal of Chemical Physics* **98** (2), 1372-1377 (1993).
32. J. P. a. B. Perdew, Kieron and Ernzerhof, Matthias, *Phys. Rev. Lett.* **77** (18), 3865-3868 (1996).
33. Y. Nie, X. Zhang, S. Ma, Y. Wang, J. Pan and C. Q. Sun, *Physical chemistry chemical physics : PCCP* **13** (27), 12640-12645 (2011).
34. R. A. Bartynski, D. Heskett, K. Garrison, G. Watson, D. M. Zehner, W. N. Mei, S. Y. Tong and X. Pan, *Journal of Vacuum Science & Technology A* **7** (3), 1931-1936 (1989).
35. T. Balasubramanian, J. N. Andersen and L. Walldén, *Physical Review B* **64** (20), 205420 (2001).
36. B. S. Fang, W. S. Lo, T. S. Chien, T. C. Leung, C. Y. Lue, C. T. Chan and K. M. Ho, *Physical Review B* **50** (15), 11093-11101 (1994).
37. B. Roldan Cuenya, J. R. Croy, S. Mostafa, F. Behafarid, L. Li, Z. Zhang, J. C. Yang, Q. Wang and A. I. Frenkel, *Journal of the American Chemical Society* **132** (25), 8747-8756 (2010).
38. E. G. Noya, J. P. K. Doye, D. J. Wales and A. Aguado, *Eur. Phys. J. D* **43** (3), 57-60 (2007).
39. J. P. K. Doye, *Computational Materials Science* **35** (3), 227-231 (2006).
40. M. Bo, Y. Wang, Y. Huang, Y. Liu, C. Li and C. Q. Sun, *Applied Surface Science* **325** (0), 33-38 (2015).

Figure captions:

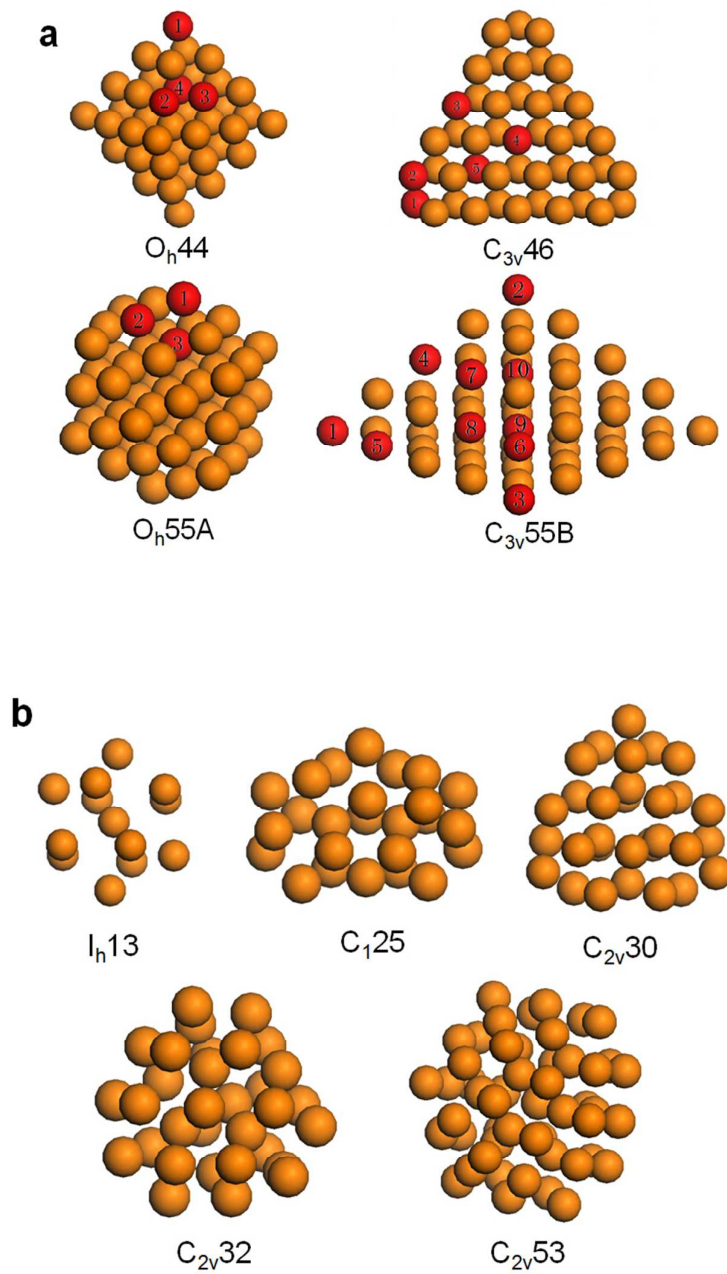


Fig. 1

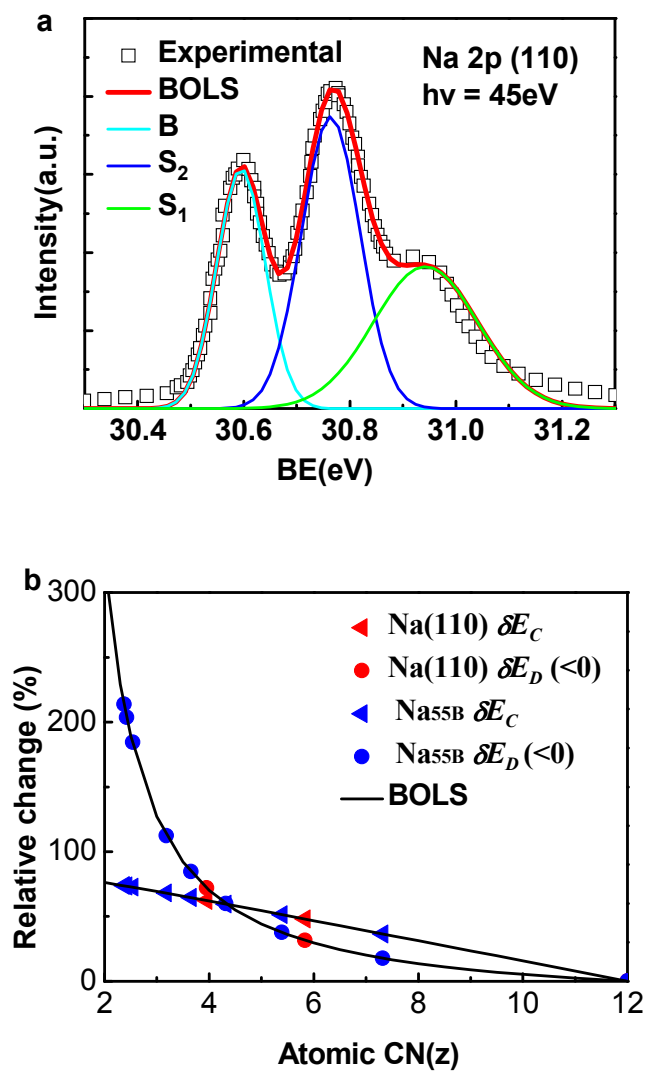
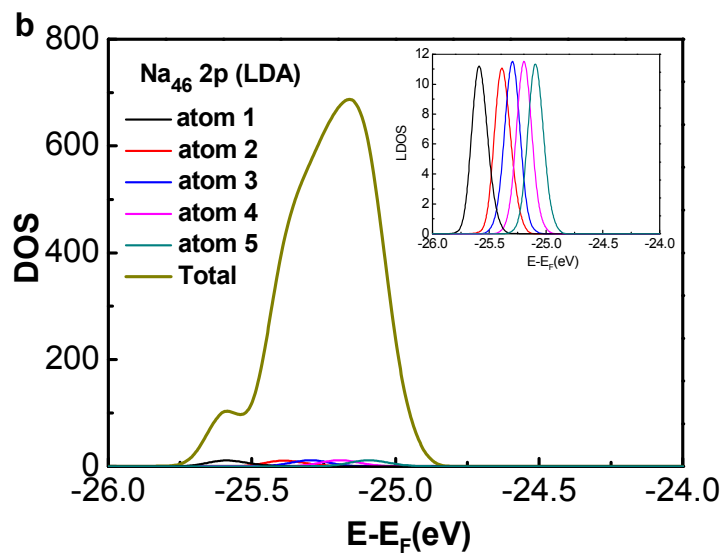
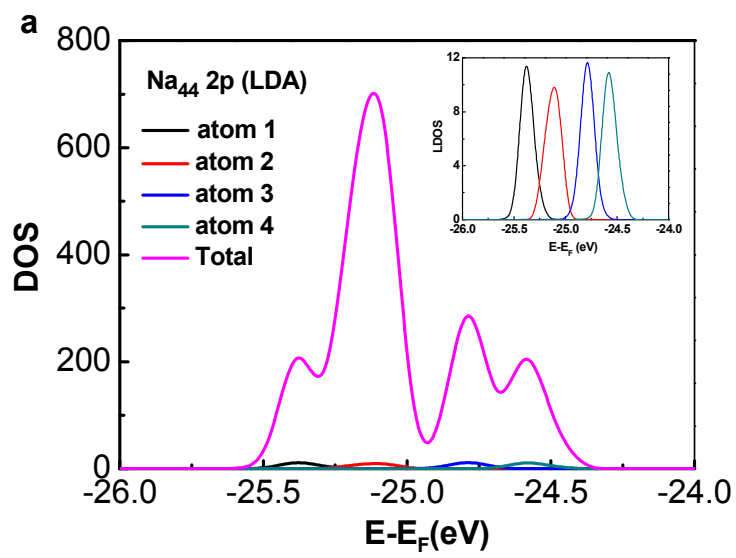


Fig. 2



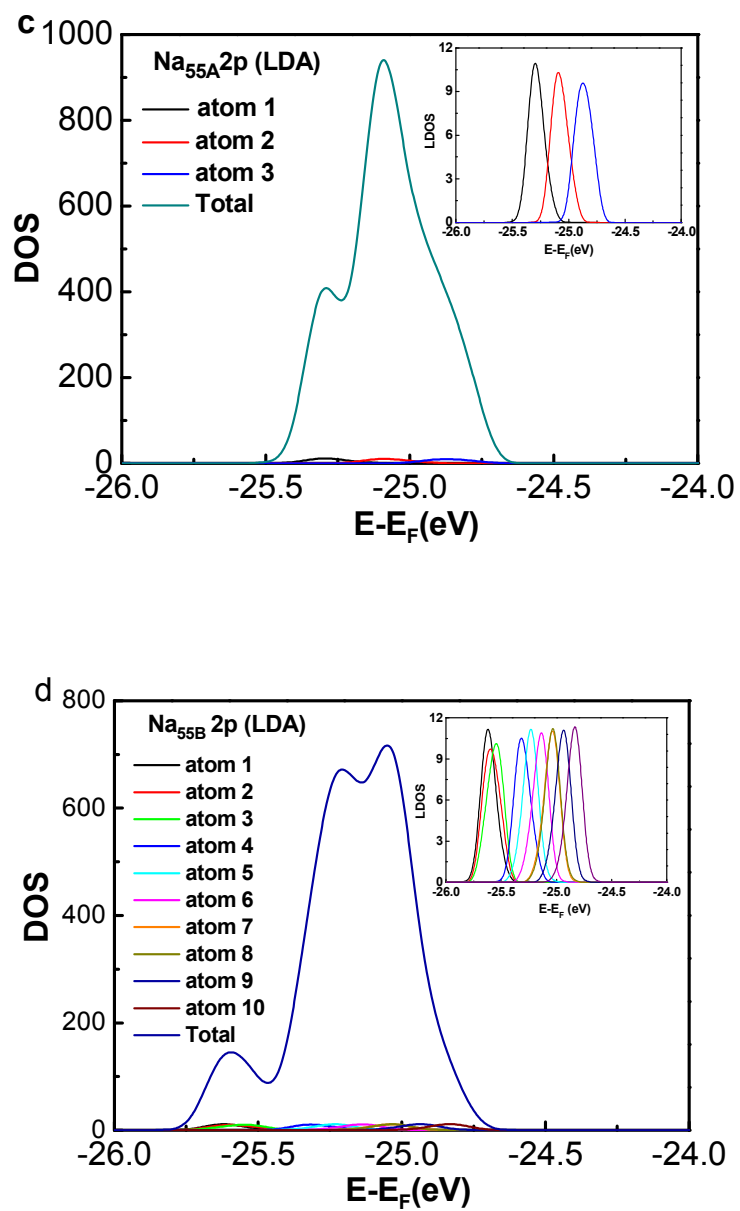


Fig. 3

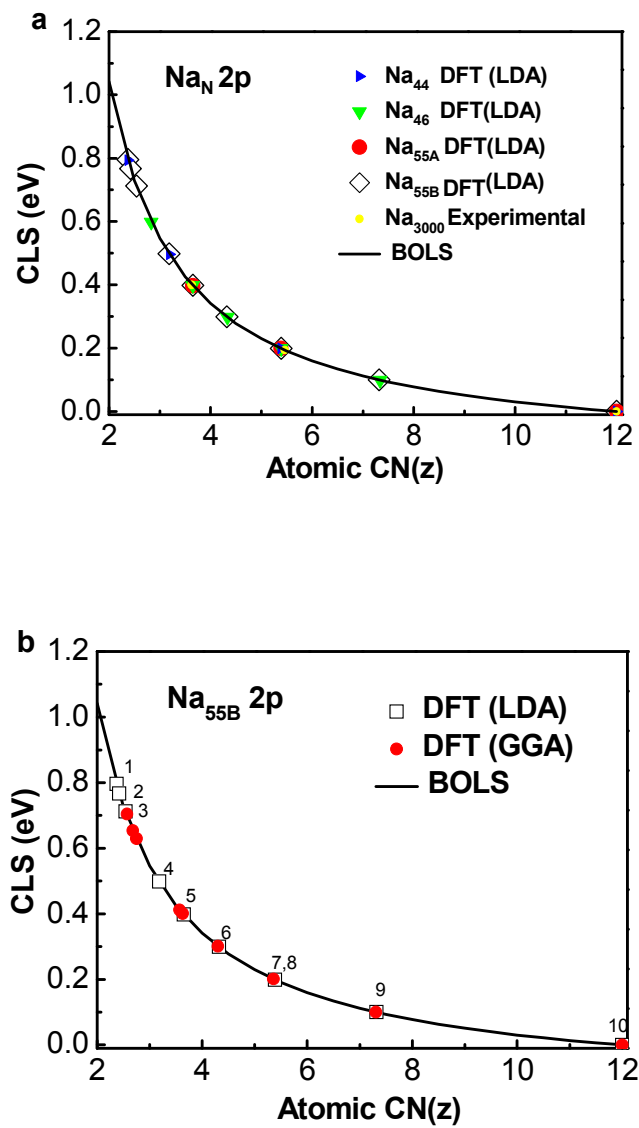


Fig. 4

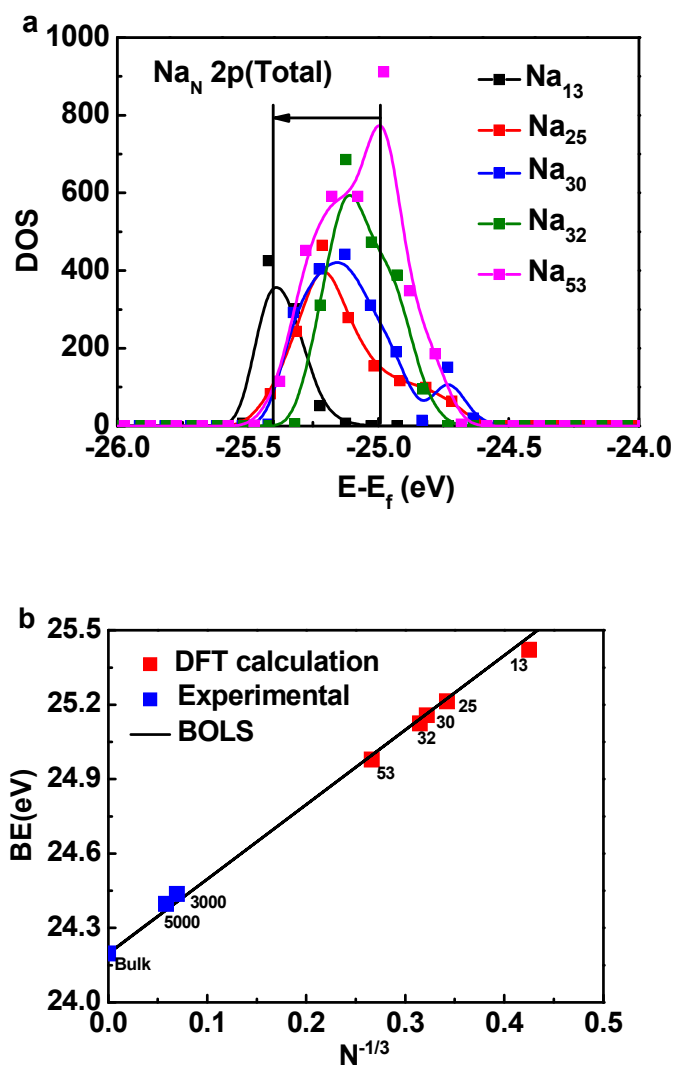


Fig. 5

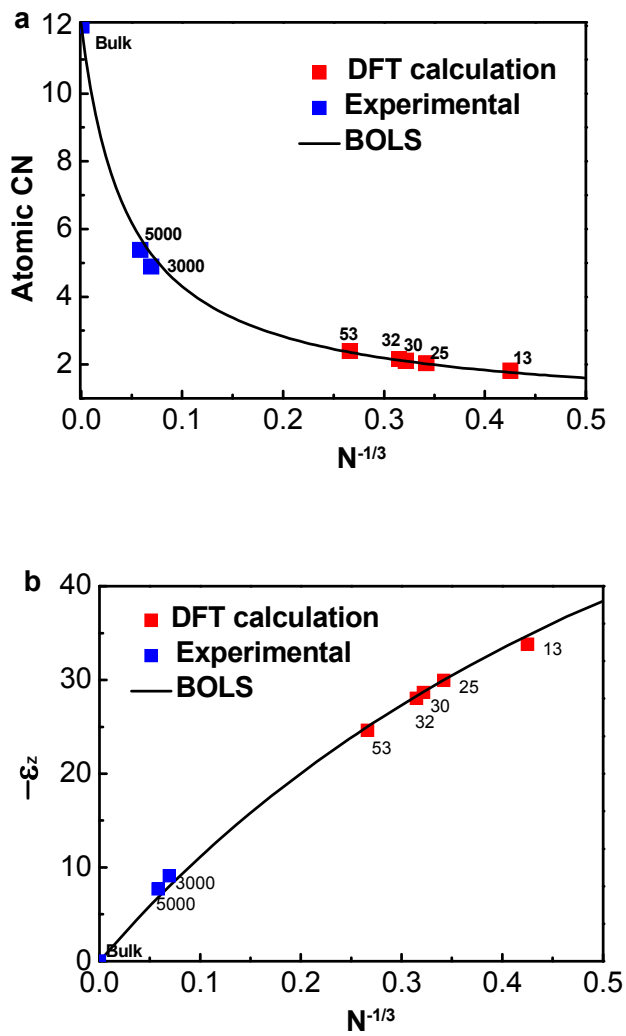


Fig. 6